ELSEVIER

PII: S0032-3861(97)10322-6

Polymer Vol. 39 No. 15, pp. 3311–3320, 1998

0032-3861/98/$19.00+0.00

TMXDI-based poly(ether urethane)/polystyrene interpenetrating polymer networks: 1. Morphology and thermal properties

Douglas J. Hourston*, Franz-Ulrich Schäfer†, John S. Bates and Michael H. S. Gradwell

Institute of Polymer Technology and Materials Engineering, Loughborough University, Loughborough, Leicestershire LE11 3TU, UK

(Received 7 November 1996; revised 22 October 1997)

In this, the first of two papers on the full composition series of simultaneous polyurethane (PUR)/polystyrene (PS) interpenetrating polymer networks (IPNs), the morphology and thermal properties are investigated. For the first time in IPN preparations, tertiary aliphatic *m*-tetramethylxylene diisocyanate (TMXDI) was used in the PUR hard segment. An investigation of the reaction kinetics of the 60:40 PUR/PS IPN composition by Fourier transform infrared (*FT*i.r.) spectroscopy, using a heated cell unit, confirmed that the PUR was the first network formed. Scanning (SEM) and transmission (TEM) electron microscopy indicated a grossly phase-separated morphology. The phase domain sizes at the outer composition ranges (90:10, 80:20, 70:30 and 10:90 PUR/PS IPNs) were smaller (20–300 nm) than at the mid-range compositions (300 nm–6 μm). SEM and TEM showed phase inversion to occur at a composition between the 30:70 and 20:80 PUR/PS IPNs. Comparing the immiscible PUR/PS IPN composition series with a similar semi-miscible PUR/PEMA IPN series revealed that in addition to phase domain sizes, the domain shape and the definition of the phase boundaries are of importance in assessing the miscibility of IPNs. No significant improvement in the thermal decomposition profile was observed for the IPN compared to the respective homonetworks.

(Keywords: interpenetrating polymer networks; morphology; scanning and transmission electron microscopy)

INTRODUCTION

An interpenetrating polymer network (IPN) is an intimate combination of two or more polymers, at least one of which is cross-linked in the presence of a network of the other. The permanent entanglements that result from the chemical (or physical) cross-links give rise to the special properties of IPNs[1–3]. Due to this forced mixing, IPN technology is a means of restricting phase separation in immiscible polymer blends and tailoring their morphology. Polyurethane (PUR) and polystyrene (PS) are highly immiscible polymers because of the polar nature of the PUR, compared to the essentially non-polar PS, and the pronounced difference in their solubility parameters[4] of $\delta = 20.5\ (\mathrm{J\ cm^{-3}})^{1/2}$ for the PUR and $\delta = 18.5\ (\mathrm{J\ cm^{-3}})^{1/2}$ for the PS. Blends of these two linear polymers, therefore, usually result in highly immiscible materials with poor mechanical properties. A number of PUR/PS IPNs[5–8] and semi-IPNs[9–11] have been studied for applications such as gas separation membranes[11–14] and damping materials[15–17]. Factors influencing the PUR/PS IPN morphology have also been investigated. These include: (i) the IPN composition[6,14], (ii) the cross-link density in both networks[6,8,11,15,18], (iii) intentionally introduced internetwork grafting[8,15] through the incorporation of difunctional monomers such as hydroxyethyl methacrylate, (iv) the presence of oppositely charged tertiary amine and carboxyl groups[19,20], and (v) the introduction of urethane acrylate-type compatibilizers into one network[15]. The influence of the synthesis conditions such as temperature[5,11,18,21], the synthesis pressure[14,22,23] and synthesis in a common solvent[7] have been investigated. Since PUR and PS are formed via two non-interfering reaction mechanisms, the simultaneous preparation method, whereby all monomers, cross-linking agents and initiators are added simultaneously, has been most commonly used. This method was also used in this study.

Most studies on PUR/PS IPNs have been conducted using diphenylmethane diisocyanate or toluene diisocyanate as part of the PUR hard segment. In this study, a tertiary, aliphatic *m*-tetramethylxylene diisocyanate (TMXDI) was used. Because of its unsymmetrical structure, crystallinity in the PUR hard segment is hindered and it would be expected to yield softer, more phase-mixed materials. While composition studies[6,14] have been conducted with PUR/PS IPNs, these rarely covered the entire composition range. In this study the entire composition range is investigated, using 10% weight increments, to determine the influence of the volume fractions on the IPN morphology. The PUR/PS IPN morphology was determined by a combination of transmission (TEM) and scanning (SEM) electron microscopy. While the former allows the determination of phase domain shapes and sizes[24], SEM is an important tool in determining the phase continuity[25–27]. Also, the morphology of the PUR/PS IPN composition series was compared with a semi-miscible PUR/PEMA IPN composition series[28]. The PUR/PEMA IPN was prepared under the same synthesis conditions, using the same PUR component. The kinetics of the IPN formation was investigated using Fourier transform infrared (*FT*i.r.) spectroscopy with a heated cell unit and the thermal properties by thermogravimetric analysis (t.g.a.). In the second paper in this series, the T_g

* To whom correspondence should be addressed
† Present address: BASF AG, D-67056 Ludwigshafen, Germany.

behaviour, mechanical properties and modulus–composition relations will be investigated.

EXPERIMENTAL

Materials and IPN preparation

The PUR component hard segment was composed of the 1,1,3,3-tetramethylxylene diisocyanate (TMXDI, kindly donated by Cytec) and the cross-linker trimethylol propane (TMP, Aldrich). The soft segment was made up of poly(oxypropylene) glycol units of a molar mass of 1025 (PPG1025, BDH). Stannous octoate (SnOc, Aldrich) was used as the PUR catalyst. Styrene monomer (S, Aldrich) was cross-linked with divinylbenzene (DVB, Aldrich) and initiated with azoisobutyronitrile (AIBN, BDH).

The IPN preparation has been described in detail in an earlier publication[15]. In brief, the TMP was dissolved in the PPG1025 at 60°C. The polymer component mixture, including the S, DVB and the dissolved AIBN, was added at room temperature. After the addition of the SnOc and the TMXDI, the components were stirred under nitrogen for 5 min. After degassing for 1 min at high vacuum, the mixture was cast in stainless steel spring-loaded O-ring moulds, which had been pre-treated with CIL Release 1711 E release agent. The curing cycle consisted of three stages: 24 h at 60°C, 24 h at 80°C and 24 h at 90°C.

IPN characterization

The kinetics of the IPN formation was investigated by *FT*i.r. spectroscopy. The equipment consisted of a Unicam *FT*i.r. spectrometer fitted with a Specac 20100 heated cell and temperature controller.

Transmission electron microscopy (TEM) was conducted for a morphological investigation of the IPNs. The elastomeric samples were embedded into Spurr's epoxy resin[29] and ultramicrotomed with a LKA Bromma 8800 Ultrotome III. Osmium tetroxide-stained and unstained samples were investigated. Staining of the 100-nm-thick sections was conducted in a 2% osmium tetroxide solution for 48 h, following the method of Kato[30]. The electron micrographs were taken with a Jeol Jem 100 CX instrument using an accelerating voltage of 60 kV.

Scanning electron microscopy (SEM) was conducted with a Leica Cambridge Stereoscan S360 instrument. The fracture surfaces were obtained from the failed tensile test specimens. These surfaces were sputtered with gold to avoid electrostatic charges and to improve image resolution.

A TG 760 Series Rheometric Scientific instrument was used to conduct the thermogravimetric analyses (t.g.a.). Samples of 4–6 mg were heated at 10°C min^{-1} in an air atmosphere.

RESULTS AND DISCUSSION

Reaction kinetics

In addition to the composition and the miscibility of the constituent network polymers, the reaction kinetics[9,31,32] of the individual components are known to have a crucial influence on the morphology and phase continuity of IPNs. In principle, three different sequences of events are possible for simultaneous IPNs: (i) polymer 1 might be formed first, or (ii) polymer 2 might be formed first, or (iii) both monomers might react simultaneously. Generally, the network that is formed first tends to have a higher degree of phase continuity[33]. With PUR/PMMA IPNs, it has been observed[34] that even materials with very similar chemistries and compositions exhibited significant differences in their morphologies. This was attributed to the difference in the order of the formation of the networks[34]. Thus, in order to investigate the influence of composition on IPN morphology and phase continuity, it was important to determine the kinetics of the IPN reactions under the given reaction conditions. The 60:40 PUR/PS IPN composition was used in this investigation.

Following the Beer–Lambert law, the concentration of the absorbing species is proportional to the area under the absorbance peak. Thus, the depletion of the isocyanate and the vinyl groups was monitored by *FT*i.r. The internal standard, to compensate for variations in sample thickness during the course of the reaction, was chosen as the combined CH_2 and CH_3 area. The integration limits for the respective functional moieties were: 2330–2160 cm^{-1} for the NCO group, 1637–1622 cm^{-1} for C=C and 3136–2810 cm^{-1} for CH_2 and CH_3. The degree of conversion, P, was determined from the following equation:

$$P(\%) = \left(\frac{C_0 - C}{C_0}\right) 100 \qquad (1)$$

Here C_0 is the initial concentration of the absorbing species and C is the concentration at any instant during the reaction. The actual temperature profile, measured in the mould by insertion of a thermocouple during a curing cycle, was mimicked in the heated cell unit. In *Figure 1* this temperature profile (solid line) is shown together with the conversion curves for both polymer networks. Under the reaction conditions used, the PUR reaction proceeded faster than the PS formation. During the latter stages of the PUR formation, a considerable amount of PS polymer had already been formed, i.e. at a PUR conversion of 75% about 25% of the PS monomer had reacted. Due to the different reaction mechanisms, linear PUR at 75% conversion would have been of an oligomeric character. However, since the PUR component was cross-linked by TMP, it is highly probable that a network had already formed at that stage and PUR gelation had taken place. At this point 25% of the styrene monomer had reacted to form polymer. The presence of PS during the formation of the PUR has been shown[9,10] to result in grossly phase-separated materials because of the mutual

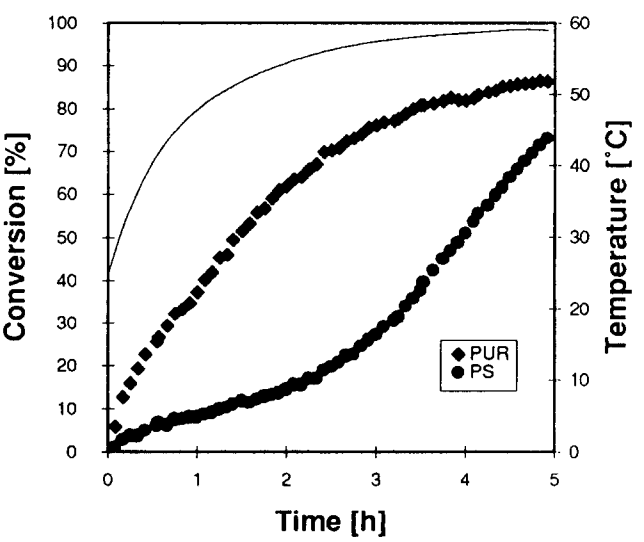

Figure 1 Percentage conversion versus time for the PUR and the PS in the 60:40 PUR/PS IPN

immiscibility of the polymers. Because of the tertiary aliphatic nature of the NCO group, the rate of PUR formation was comparatively slow. A more reactive NCO group such as in an aromatic diisocyanate might, therefore, have resulted in less phase-separated IPNs.

Morphology

The visual appearance of the 3-mm-thick IPN sheets indicated a phase-separated morphology with only the pure PUR and PS networks being transparent. Some degree of

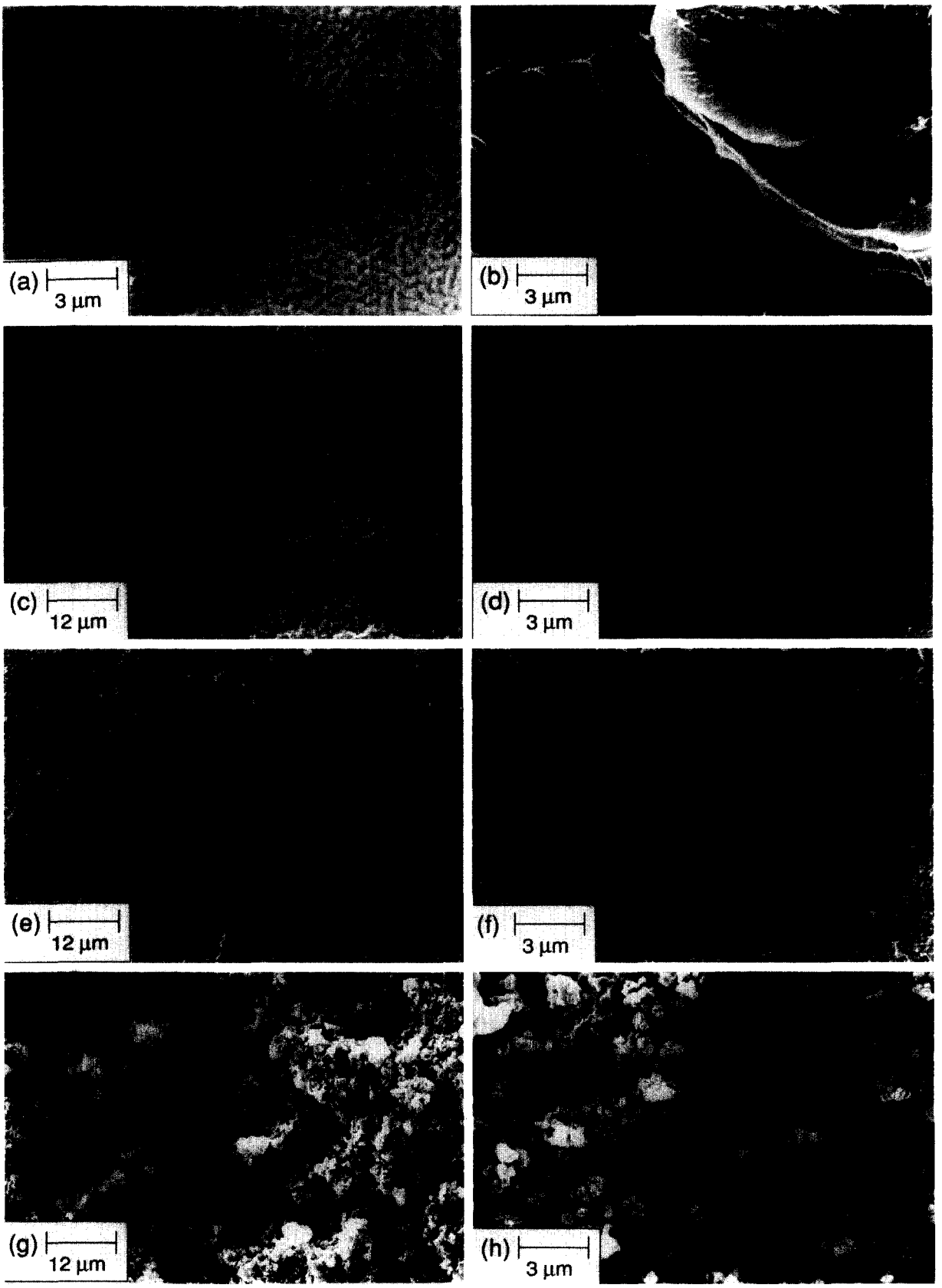

Figure 2 Scanning electron micrographs for different PUR/PS compositions: (a) pure PUR, (b) pure PS, (c) and (d) 80:20 PUR/PS, (e) and (f) 70:30 and (g) and (h) 60:40

transparency was still present at PUR levels of 90 and 80%, indicating that the PS domains were smaller than the wavelength of visible light. The opacity observed at the other compositions is characteristic[9] of phase-separated materials and this criterion has been used[8] to study the phase separation in PUR/PS IPNs. Electron microscopy was used to investigate further the IPN morphology. While TEM provides two-dimensional information only, SEM can give some insight into topographic features of a fracture surface[24], thus complementing TEM[35]. Broken tensile test

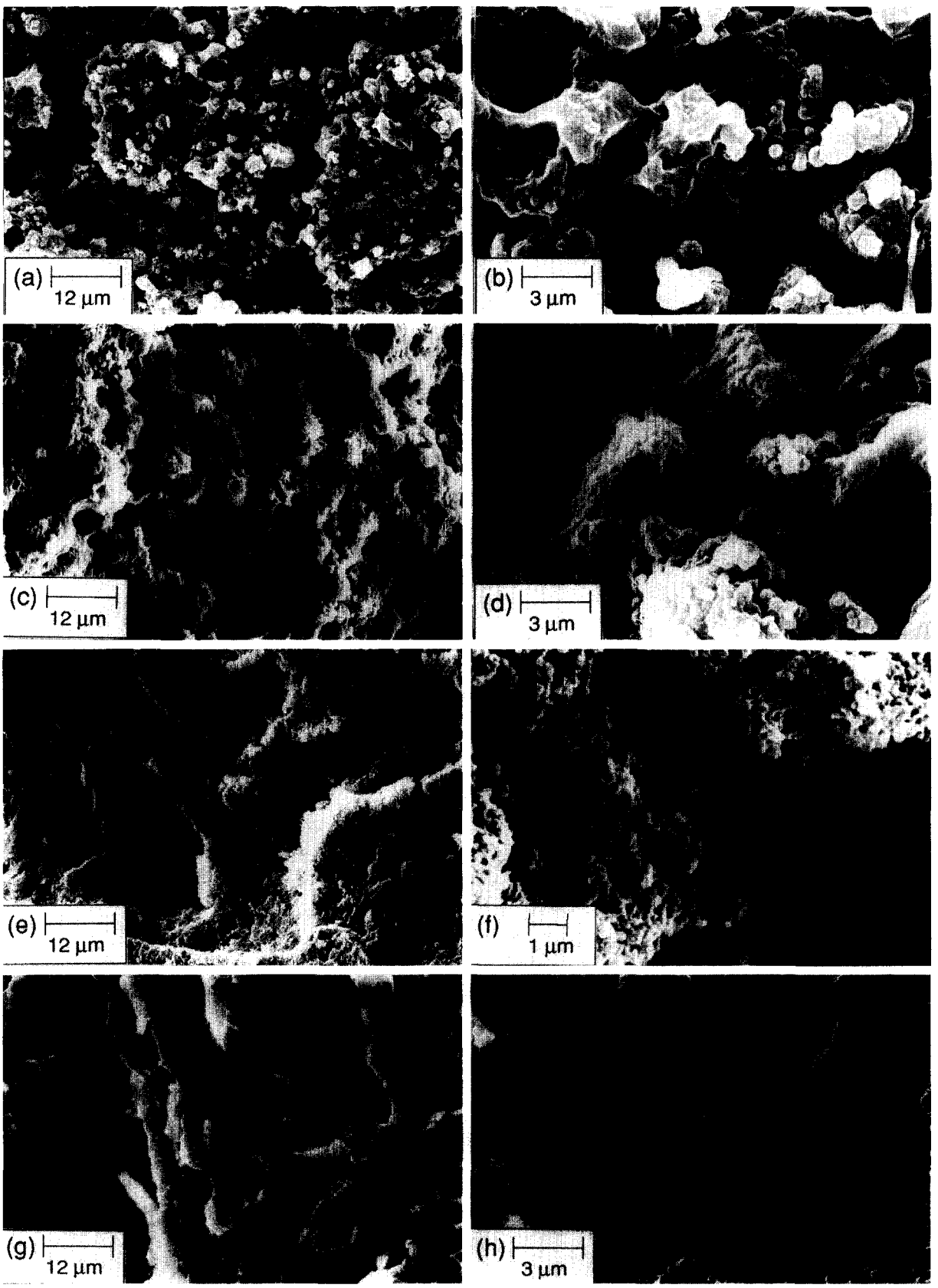

Figure 3 Scanning electron micrographs for different PUR/PS compositions: (a) and (b) 40:60 PUR/PS, (c) and (d) 30:70, (e) and (f) 20:80 and (g) and (h) 10:90

specimens were used for the SEM investigation. Tensile tests were conducted at room temperature, above the glass transition of the PUR network (−34°C) and below that of the PS network (100°C), at a cross-head speed of 50 mm min^{-1}. Because of the different failure behaviour of the two materials at room temperature, separate phases or inhomogeneities in the IPN were expected to become readily visible. The scanning electron micrographs are shown in *Figures 2* and *3*. The micrograph of the pure PUR network exhibited a clean fracture pattern (*Figure 2a*). The surface structure that appeared on this micrograph was not investigated, but is probably the result of sample preparation rather than an indication of hard and soft segment segregation within the PUR. The scanning electron micrograph of the pure PS showed brittle failure with little surface structure present (*Figure 2b*). The effect of increasing the PS weight fraction in the PUR is shown by SEM (*Figures 2* and *3*) and TEM (*Figures 4* and *5*). The scanning electron micrograph of the 80:20 PUR/PS IPN showed a fairly homogeneous fracture surface at a low magnification of 5000 (*Figure 2c*). At a magnification of 20000, a PUR matrix with small PS domains of 50–200 nm was observed (*Figure 2d*). At the 70:30 composition (*Figure 2e*), a rougher surface structure was noted at a magnification of

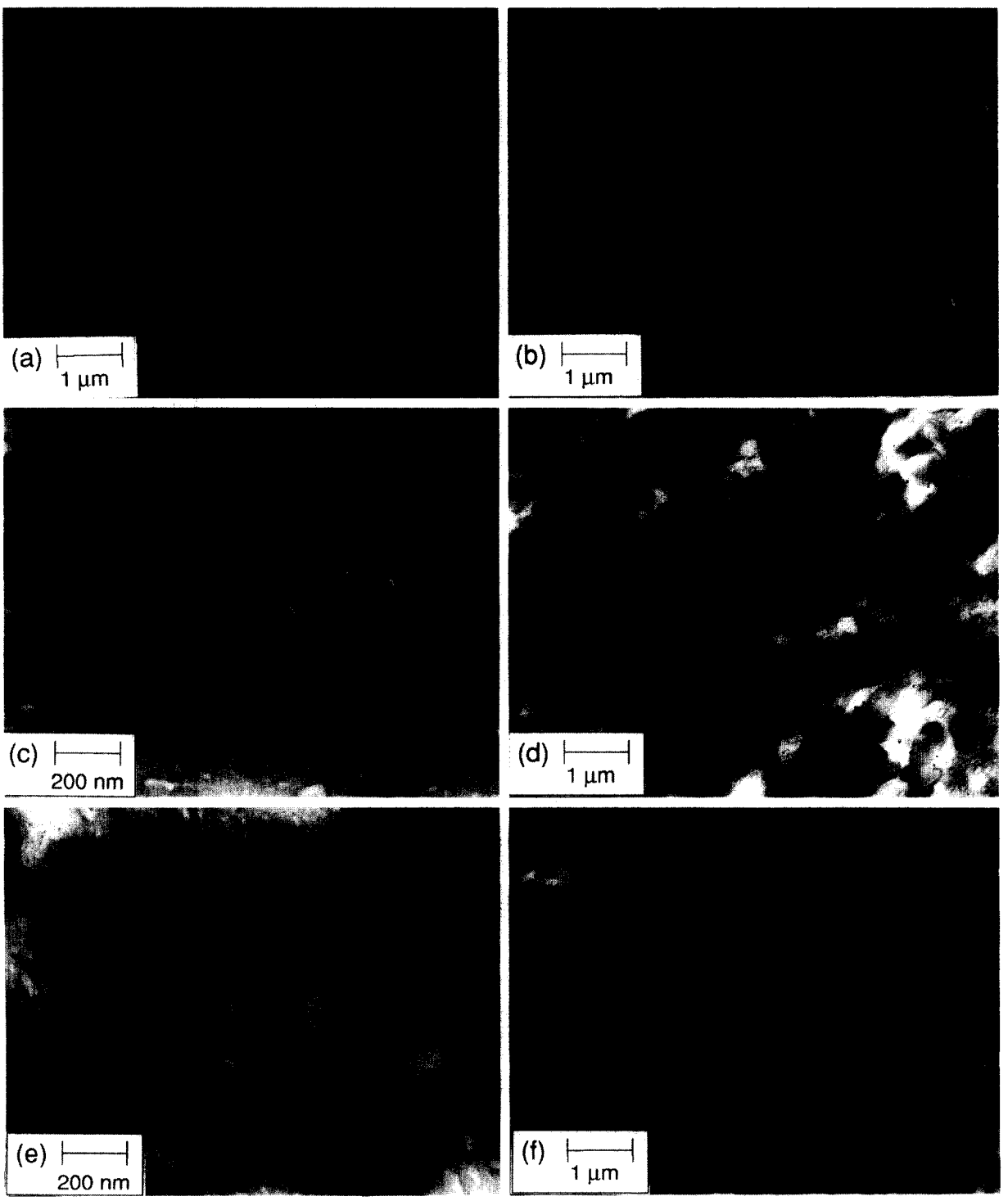

Figure 4 Transmission electron micrographs for different PUR/PS IPN compositions: (a) 80:20 PUR/PS, (b) and (c) 70:30, (d) and (e) 60:40 and (f) 60:40, unstained

5000. At 20 000 (*Figure 2f*), the PS domains also increased in size to 100–300 nm. The scanning electron micrographs of the 60:40 PUR/PS IPN composition (*Figure 2g* and *h*) showed the same trend, yet much more pronounced. The fracture surface exhibited a highly irregular structure at a magnification of 5000 and the domain size increased even further to 200–800 nm. In addition to these larger domains, cylinder-shaped cavities were observed in the matrix (*Figure 2h*). The presence of cavities and the comparatively large domain sizes indicated that phase mixing and cohesion between the PUR and PS phases was poor. At this 60:40 composition, the PS network exhibited a limited degree of local phase continuity, but it was believed that the PUR network still constituted the matrix. The cavities observed at compositions from the 60:40 to the 40:60 PUR/PS IPNs were, most likely, PS-rich cylindrical domains. *Figure 2h* shows the effect of using the back-scattered electron mode. Back-scattered electrons[36] are primary beam electrons that have been elastically scattered by the nuclei in the sample and escape from the surface. On the left of the micrograph is the secondary electron image and on the right the back-scattered electron image after staining the sample with osmium tetroxide[30]. A maximum in the number of structural irregularities and cylindrical cavities was observed for the

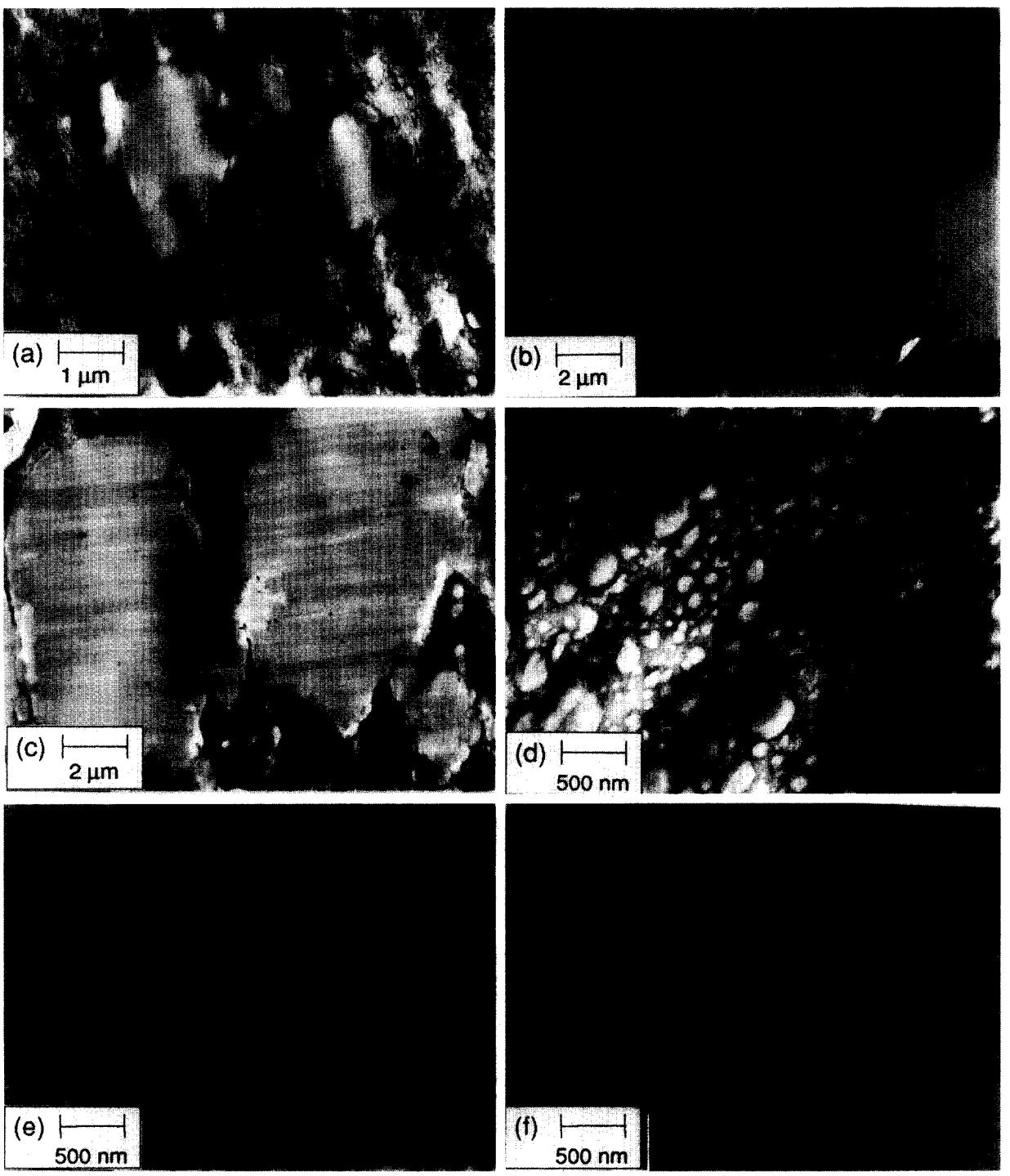

Figure 5 Transmission electron micrographs for different PUR/PS compositions: (a) 50:50 PUR/PS, (b) 40:60, (c) and (d) 30:70 PUR/PS, (e) 20:80 and (f) 10:90

40:60 composition (*Figure 3a*). Also, the domain size was the largest with diameters of 600 nm to 4 μm (*Figure 3b*). At the 30:70 PUR/PS composition (*Figure 3c*), an important change in IPN morphology was observed from the fracture surface. Clearly, fewer and shallower cavities were observed although the fracture surface still appeared very rough (*Figure 3d*). This was considered to be the beginning of phase inversion to a predominantly PS-matrix. At the 20:80 PUR/PS IPN composition (*Figure 3e*), the cylindrical cavities had completely disappeared. At a magnification of 5000, the surface structure showed similarities to the pure PS fracture surface. At 50 000, however, a fine morphology of small interconnected cylinders of 100–150 nm in diameter was noted (*Figure 3f*). The 10:90 composition exhibited an even finer morphology (*Figure 3g*). The interconnected cylinders were no longer evident and numerous very small, probably PUR-rich domains of about 50–100 nm diameter appeared. Thus, from the scanning electron micrographs, a two-phase morphology with gross phase separation was observed. Three different structures were noted, and upon increasing the PS content to the 70:30 PUR/PS IPN composition, a fairly regular fracture surface was obtained, with domain size increasing with higher PS content. The 60:40 to 30:70 compositions had a highly irregular fracture surface which showed the presence of large cylindrical cavities. The latter indicating some degree of local phase continuity of the PS phase with, however, poor adhesion between both phases. The 20:80 and 10:90 compositions exhibited a smoother fracture surface having some resemblance to that of pure PS, PS being believed to represent the continuous phase.

Transmission electron micrographs (*Figures 4* and *5*) were taken to elucidate further the IPN morphology, in particular the phase domain size and shape and the interfacial area. Even though an indication of phase domain sizes could be obtained from the SEM studies, these estimations were limited because of the difficulty in determining the exact borders of the phase domains and the relatively low magnifications. Osmium tetroxide preferentially stains the ether linkages of the PUR soft segment[2], thus the darker regions in the transmission electron micrographs consist of PUR or have[10] a high PUR content. A micrograph of the osmium tetroxide-stained pure PUR showed no microstructure as a result of hard and soft segment segregation. This confirmed that PURs prepared from TMXDI-based hard segments have little tendency to phase segregate. TEM studies[37] of phase-segregated MDI-based PURs have revealed microphase separation with hard segment domain sizes in the order of 10–20 nm. The transmission electron micrograph of the 80:20 PUR/PS IPN composition showed many very small PS phase domains of 10–100 nm in diameter (*Figure 4a*). The PS phase domains appeared darker than the matrix due to a darkly-stained shell which surrounded them. In a recent study, He *et al.*[10] investigated a 30:70 PUR/PS IPN by SEM. Selective degradation of the PUR by treatment with an ethanolic sodium hydroxide solution revealed the existence of a shell surrounding the PS domains. This shell contained[10] more PUR than the matrix since no obvious degradation could be observed for the latter. A model to explain the development of the PUR/PS morphology was proposed and a concentration curve going from the noduli towards the matrix was presented[10]. This high-purity PUR shell surrounding the PS domains was clearly evident in the transmission electron micrographs of this study (*Figures 4* and *5*), thus confirming the theory of He *et al.*[10]. It also indicated that the IPN matrix did not consist of pure PUR, but that it had some PS dissolved in it. *Figures 4b* and *c* shows micrographs of the 70:30 PUR/PS IPN. The phase domain sizes clearly increased to values between 20 and 200 nm, while the phase domain sizes in the 80:20 IPN were smaller and fairly uniform (*Figure 4a*). Some larger phase domains of up to 400 nm were found in the 70:30 PUR/PS IPN (*Figure 4b*) and other samples with decreasing PUR contents. This was explained[7] by the combined effect of a decreased rate of PUR network formation and a decreased viscosity of the medium, both of which favour phase separation. A further PS phase domain size increase was observed in the 60:40 PUR/PS IPN. *Figure 4d* and *e* showed a distribution of PS phase domain sizes with numerous smaller domains of about 50–200 nm and a few larger domains in the order 400–700 nm. Many domains had an ellipsoidal shape, almost certainly an indication of the existence of the cylindrical cavities that were observed by SEM (*Figures 2h* and *3b*). The darkly-stained PUR was believed to have constituted the continuous phase at this composition since no pronounced change in morphology was observed. Again, dark-stained shells surrounding PS phase domains were evident (*Figure 4e*). The numerous small black particles in this micrograph were staining artefacts, resulting from osmium tetroxide or osmium dioxide crystals. Some degree of electron contrast was present in an unstained 60:40 PUR/PS sample (*Figure 4f*); however, the phase contrast was poorer than in the stained counterpart (*Figure 4d*). In the unstained IPN, the PS domains appeared darker than the PUR matrix, indicating that the electron density of the PS was higher than that of the PUR. Also, within the lighter PUR matrix variations were noted similar to those in some stained transmission electron micrographs. These are indicative of variations in the PS content that was dissolved in the predominantly PUR matrix. These darker matrix regions were more frequently observed around agglomerates of PS domains and appeared to be to some extent interconnected. This could be an indication that as the PS polymerized, first spheres and then cylindrical PS-rich domains formed, indicating a change from a nucleation and growth to a spinodal decomposition phase separation mechanism. A similar phenomenon was noted[2] for a polybutadiene/PS IPN; however, it must be emphasized that the variations in matrix darkness could also be due to slight variations in sample film thickness. With increasing PS content, larger PS phase domains appeared (*Figure 5*). At the 50:50 PUR/PS IPN composition a distribution of small (100–200 nm) and larger (500–700 nm) PS domains was observed (*Figure 5a*). In addition to these, numerous PS domains of 1–3 μm also appeared. This trend was continued with the 40:60 composition (*Figure 5b*), where a distribution of small PS domains still observed, as well as larger domains in the order of 2–6 μm. At the 30:70 composition, even larger PS domains were noted (*Figure 5c*). It was no longer clear which phase represented the continuous phase as even the volume fraction of the PS domains appeared to be greater than the area of the PUR enriched phases, the latter still appeared more continuous. *Figure 5d*) shows that very small PS phase domains of 50–400 nm were present. A dramatic change in IPN morphology was observed at the 20:80 PUR/PS IPN composition. This composition showed predominantly interconnected PS phases (*Figure 5e*) and in between the light PS phase, dark worm-like domains of a PUR/PS blend were observed. Thus, from the transmission electron micrographs, it appeared that phase inversion had occurred between the

30:70 and 20:80 PUR/PS compositions. The morphology of the 20:80 composition, as observed by TEM, had a strong resemblance to the worm-like interconnected structures that were observed by SEM (*Figure 3f*). The 10:90 composition showed a poorly resolved morphology with very small dark PUR domains of 30–80 nm in diameter.

Comparing the scanning and transmission electron micrographs of the PUR/PS IPNs to those of a semi-miscible PUR/PEMA IPN composition series[17,28] prepared with the same PUR network and under the same reaction conditions revealed some distinct differences in IPN morphology for some compositions. From the scanning electron micrographs, no significant difference in morphology could be observed for the outer compositions (90:10, 80:20, 70:30 and 10:90) between the PUR/PS and the PUR/PEMA IPNs. However, for the inner compositions (60:40 to 30:70), the scanning electron micrographs of the PUR/PEMA IPNs [17] showed a much smoother fracture surface (*Figure 6a*). The latter indicated that at the inner compositions the PUR/PS IPNs had larger phase domain sizes and that the interfacial adhesion was poor. At the outer composition series, SEM studies were not a sensitive enough tool to differentiate between the two types of IPNs. With TEM, however, a notable difference existed between, for example, the 70:30 PUR/PS (*Figure 4b* and *c*) and the 70:30 PUR/PEMA (*Figure 6b* and *c*) IPNs. While the phase domain sizes were roughly similar for both types of IPNs (between 20 and 200 nm), their shape and the interface region were clearly different. The PS domains were spherical (ellipsoidal) and their phase boundaries were well-defined by a dark shell. The PEMA domains, on the other hand, were very irregularly shaped. No definite phase boundaries could be observed to the extent that the PEMA phases appeared to be continuous to some degree. Various shades of grey (stemming from different dark-stained PUR contents) at the phase boundaries suggested the presence of a well-mixed interface. Thus, this comparison suggests that rather than paying attention to phase domain sizes in IPNs, more importance has to be placed on phase domain shape, the definition of the phase boundaries and the interface area when assessing IPN miscibility from transmission electron micrographs. At the 40:60 PUR/PEMA IPN composition (*Figure 6d*) phase inversion had already occurred and dark PUR-rich domains of 100–200 nm were observed in a white PEMA-rich matrix, whereas in the 40:60 PUR/PS IPN a distribution of large PS domains (6 μm) was present in a PUR-rich matrix (*Figure 5b*). Thus, phase inversion took place at a higher high T_g polymer content in the immiscible PUR/PS IPNs (70–80% PS) than in the semi-miscible PUR/PEMA IPNs (60–50% PEMA).

Thermal analysis

Thermogravimetric analysis (t.g.a.) can be employed[38] to assess the thermal stability and decomposition temperature and to study the decomposition mechanism and products of polymers[39]. In a t.g.a. study on IPNs, Kim *et al.*[40] found improved thermal properties for a PUR/PMMA IPN. They concluded that the depolymerizing MMA acted as a radical scavenger and improved the thermal stability of the PUR. The same authors[41] reported a higher weight retention of the PUR/PS IPNs, above 400°C, compared to the respective homopolymers. Kim and Kim[7] also found an enhancement of thermal stability in PUR/PS IPNs. This enhancement was more pronounced in IPNs that had been synthesized in the presence of a common solvent, a fact that they attributed to a higher degree of interpenetration in these IPNs. T.g.a. studies of selected PUR/PS IPN compositions were conducted, the percentage weight loss *versus* temperature

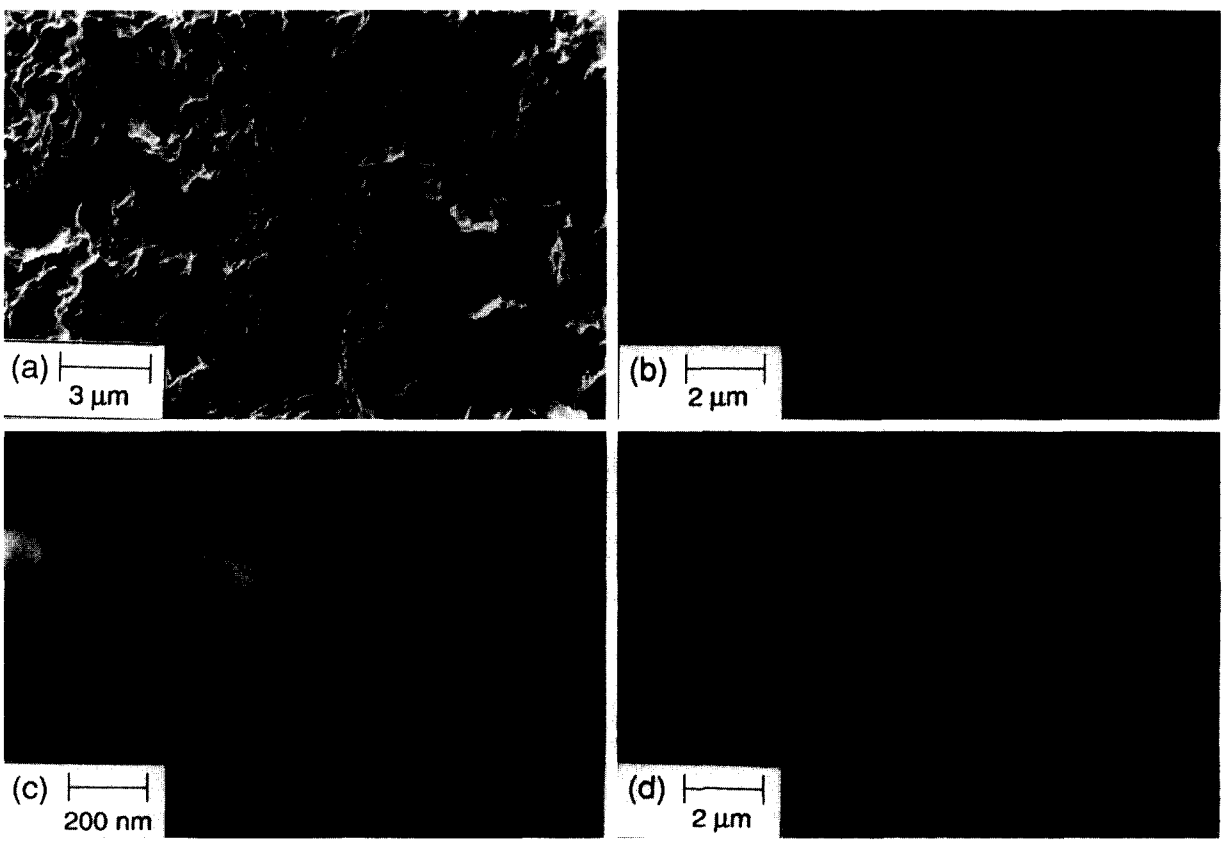

Figure 6 Scanning electron (a) and transmission electron (b–d) micrographs of PUR/PEMA IPN compositions: (a) 50:50, (b) and (c) 70:30 and (d) 40:60

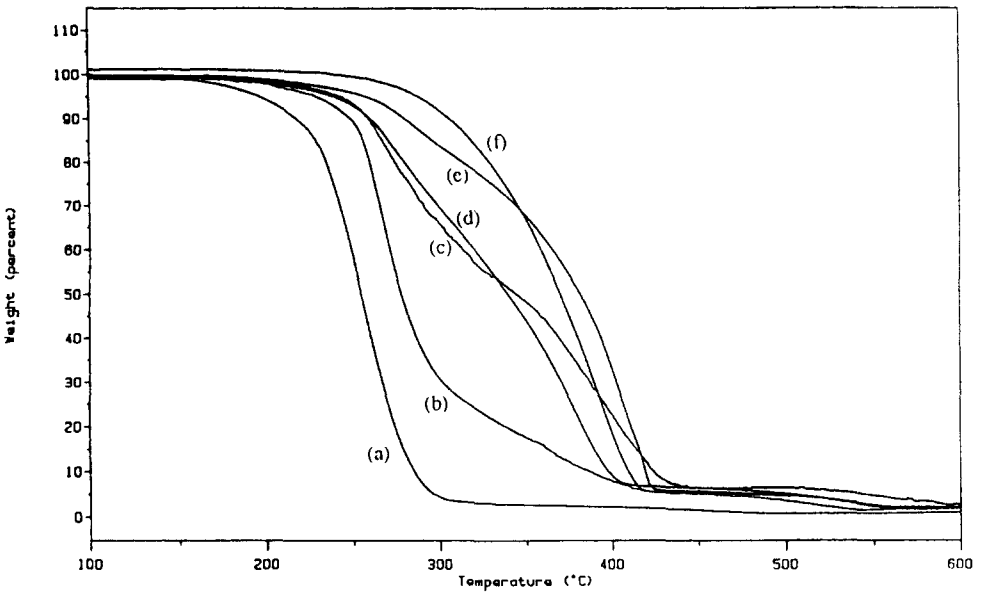

Figure 7 Percentage weight loss versus temperature for PUR/PS IPN compositions: (a) pure PUR, (b) 80:20 PUR/PS, (c) 60:40, (d) 40:60 (e) 20:80 and (f) pure PS

data are shown in *Figure 7*. Whilst the previously mentioned studies were conducted in a nitrogen atmosphere, in this study an air atmosphere was used in order to simulate better environmental conditions. The PUR was found to have the poorest thermal stability (*Figure 7a*). A considerable weight loss started to occur at 230°C and at 300°C less than 5% of the initial weight remained. The three main decomposition reactions for PURs are[39] (i) the dissociation into the isocyanate and the alcohol, (ii) the formation of a primary amine, CO_2 and an olefin and (iii) the formation of a secondary amine and carbon dioxide. While the dissociation into the isocyanate and alcohol can occur[39] at temperatures as low as 140°C, there was no evidence of this reaction from the t.g.a. curve. The latter two reactions are known[39] to occur above 200°C as was seen in the t.g.a. curve. The 80:20 PUR/PS IPN composition exhibited a better thermal stability than the pure PUR (*Figure 7b*). The major weight loss only started to occur at 260°C and a two-stage drop was observed. A rapid weight loss down to 30% over a temperature range of 30°C was followed by a more gradual weight loss to 5% over a range of 110°C. This corresponded to some extent to the weight percentages of PUR and PS present in the IPN. The pure PS network had a much better thermal stability and significant weight loss only started to occur at temperatures above 300°C (*Figure 7f*). The weight loss proceeded in an essentially one-step drop down to 3% weight retention. The 60:40 and 40:60 compositions had similar thermal property profiles (*Figures 7c* and *d*). The 20:80 PUR/PS composition showed a surprising phenomenon (*Figure 7e*). While a weight loss of the first 25% occurred at temperatures lower than the PS decomposition, the remaining 75% were lost at temperatures higher than those of the pure PS polymer. This was similar to the findings of Kim *et al.*[41] who observed a higher weight retention above 400°C for PUR/PS IPNs. Thus, the thermogravimetric analyses in an air atmosphere showed that, compared to pure PUR, the IPNs showed some improvement in the thermal properties. However, very limited synergism of the thermal properties of the IPNs was observed and for most of the compositions the curves exhibited mere averages of the constituent PUR and PS homonetworks. Similar results of a two-step weight loss were obtained when analysing the semi-miscible PUR/PEMA IPN[42]. In the PUR/PEMA IPN[42], an improved thermal stability was obtained with an increase in cross-link density in the PUR network.

CONCLUSIONS

*FT*i.r. studies of the 60:40 PUR/PS IPN confirmed that the PUR network was formed first under the reaction conditions used. By combining SEM and TEM studies the morphology of the PUR/PS IPN composition series was characterized. Clear phase separation over the entire composition series was observed from the transmission and scanning electron micrographs. The PS phase domain sizes as observed from TEM varied from 20 to 300 nm at the outer PUR/PS IPN composition ranges (90:10, 80:20, 70:30 and 10:90) from 300 nm to 8 μm at the mid-composition ranges (60:40 to 20:80). In the stained IPN samples, the PS domains were surrounded by a dark PUR-rich shell. The PS domains in the 90:10 to the 30:70 PUR/PS IPN compositions were spherical and ellipsoidal in shape. The ellipsoidal PS domains were found in the scanning electron micrographs in form of cylindrical cavities. Scanning and transmission electron micrographs showed phase inversion from a predominantly PUR-rich to a PS-rich matrix taking place between the 30:70 and 20:80 PUR/PS IPN compositions. Comparing the immiscible PUR/PS IPN composition series with a similar semi-miscible PUR/PEMA IPN series revealed that in addition to phase domain sizes, the domain shape and the definition of the phase boundaries were of great importance when assessing the miscibility of the IPNs. Phase inversion occurred at lower PUR contents in the immiscible PUR/PS IPN series (30 to 20% PUR) than in the semi-miscible PUR/PEMA IPNs (60 to 50% PUR). No significant improvement in the thermal decomposition profile was observed for the IPNs when compared to the respective PUR and PS homonetworks.

ACKNOWLEDGEMENTS

One of the authors (F.-U. S.) would like to acknowledge a

grant from the German Academic Exchange Service, Deutscher Akademischer Austauschdienst DAAD.

REFERENCES

1. Klempner, D. and Berkowski, L., in *Encyclopedia of Polymer Science and Engineering*, Vol. 8, ed. H. Mark, N. M. Bikales, C. G. Overberger and G. Menges. Wiley, New York, 1988.
2. Sperling, L. H., in *Interpenetrating Polymer Networks*, ACS 239, ed. D. Klempner, L. H. Sperling and L. A. Utracki. ACS, Washington, DC, 1994.
3. Sperling, L. H., *Interpenetrating Polymer Networks and Related Materials*. Plenum Press, New York, 1981.
4. Brandrup, J. and Immergut, E. H. (ed.), *Polymer Handbook*, 3rd edn. Wiley, New York, 1989.
5. Kim, B. S., Lee, D. S. and Kim, S. C., *Macromolecules*, 1986, **19**, 2589.
6. Kim, S. C., Klempner, D., Frisch, K. C., Frisch, H. L. and Ghiradella, H., *Polym. Eng. Sci.*, 1975, **15**, 339.
7. Kim, S. K. and Kim, S. C., *Polym. Bull.*, 1990, **23**, 141.
8. Nevissas, V., Widmaier, J.-M. and Meyer, G. C., *J. Appl. Polym. Sci.*, 1988, **36**, 1467.
9. He, X., Widmaier, J.-M. and Meyer, G. C., *Polym. Int.*, 1993, **32**(3), 289.
10. He, X., Widmaier, J.-M. and Meyer, G. C., *Polym. Int.*, 1993, **32**(3), 295.
11. Lee, D. S., Jung, D. S., Kim, T. H. and Kim, S. C., *J. Membrane Sci.*, 1991, **60**, 233.
12. Lee, D. S., Kang, W. K., An, J. H. and Kim, S. C., *J. Membrane Sci.*, 1992, **75**, 15.
13. Lee, D. S. and Kim, S. C., *Macromolecules*, 1984, **17**, 2222.
14. Lee, D. S. and Kim, S. C., *Macromolecules*, 1985, **18**, 2173.
15. Hourston, D. J. and Schäfer, F.-U., *Polym. Adv. Technol.*, 1996, **7**, 273.
16. Hourston, D. J. and Schäfer, F.-U., *High Perform. Polym.*, 1996, **8**, 19.
17. Schäfer, F.-U., Ph.D. Thesis, Loughborough University, Loughborough, UK, 1996.
18. Lee, D. S. and Park, T. S., *J. Appl. Polym. Sci.*, 1991, **43**, 481.
19. Hsieh, K. H. and Chou, L. M., *J. Appl. Polym. Sci.*, 1989, **38**, 645.
20. Hsieh, K. H., Chou, L. M. and Wong, S. S., *Angew. Makromol. Chem.*, 1989, **168**, 145.
21. Lee, D. S. and Park, T. S., *Polym. J.*, 1991, **23**, 241.
22. Lee, D. S. and Kim, S. C., *Macromolecules*, 1984, **17**, 2193.
23. Lee, L. H. and Kim, S. C., *Macromolecules*, 1986, **19**, 644.
24. Thomas, D. A., in *Advances in Preparation and Characterization of Multiphase Polymer Systems*, ed. R. J. Ambros and S. L. Aggarwal. Wiley, New York, 1978.
25. An, J. H. and Sperling, L. H., in *Cross-linked Polymers*, ACS Symposium Series 367. American Chemical Society, Washington DC, 1988.
26. Widmaier, J.-M. and Sperling, L. H., *Macromolecules*, 1982, **15**, 625.
27. Sperling, L. H. and Widmaier, J.-M., *Polym. Eng. Sci.*, 1983, **23**, 694.
28. Hourston, D. J. and Schäfer, F.-U., *Polymer*, 1996, **37**, 3521.
29. Spurr, A. R., *J. Ultrastructure Res.*, 1969, **26**, 31.
30. Kato, K., *Polym. Eng. Sci.*, 1967, **1**, 38.
31. Djomo, H., Morin, A., Damyanidu, M. and Meyer, G. C., *Polymer*, 1983, **24**, 65.
32. Lipatov, Y. S., Semenovitch, G. M., Skiba, S. I., Karabanova, L. V. and Sergeeva, L. M., *Polymer*, 1992, **33**, 361.
33. Donatelli, A. A., Sperling, L. H. and Thomas, D. A., *J. Appl. Polym. Sci.*, 1977, **21**, 1189.
34. Sperling, L. H. and Mishra, V., *Polym. Adv. Technol.*, 1996, **7**, 197.
35. Sawyer, L. C. and Grupp, D. T., *Polymer Microscopy*. Chapman and Hall, London, 1987.
36. Wischnitzer, S., *Introduction to Electron Microscopy*, 3rd edn. Pergamon Press, New York, 1980.
37. Oertel, G., *Polyurethane Handbook*, 2nd edn. Carl Hanser, Munich, 1994.
38. Billmeyer, F. W., *Textbook of Polymer Science*, 3rd edn. Wiley, New York, 1984.
39. Odian, G. G., *Principles of Polymerization*, 3rd edn. Wiley Interscience, 1991.
40. Kim, S. C., Klempner, D. and Frisch, K. C., *J. Appl. Polym. Sci.*, 1977, **21**, 1289.
41. Kim, S. C., Klempner, D., Frisch, K. C., Frisch, H. L. and Ghiradella, H., *Polym. Eng. Sci.*, 1975, **15**, 339.
42. Hourston, D. J. and Schäfer, F.-U., *J. Appl. Polym. Sci.*, 1997, **62**, 2025.